RESEARCH ARTICLE | MAY 23 2023

Halloysite nanotube loaded polyamide nanocomposites: Structural, morphological, mechanical, thermal and processing behaviors

Alinda Öykü Akar; Ümit Hakan Yıldız; Ümit Tayfun

AIP Conference Proceedings 2607, 070005 (2023)
https://doi.org/10.1063/5.0135873

Halloysite Nanotube Loaded Polyamide Nanocomposites: Structural, Morphological, Mechanical, Thermal and Processing Behaviors

Alinda Öykü Akar[1, a)], Ümit Hakan Yıldız[2, 3, b)] and Ümit Tayfun[3, 4, c)]

[1]*Eczacıbasi Esan, R&D Center, Istanbul, Turkey*
[2]*Izmir Institute of Technology, Chemistry Department, Izmir, Turkey*
[3]*Inovasens Ltd, Izmir Technopark, Izmir, Turkey*
[4]*Department of Basic Sciences, Bartin University, Bartin, Turkey*

[a)] a.akar@gtu.edu.tr
[b)] hakanyildiz@iyte.edu.tr
[c)] Corresponding author: utayfun@bartin.edu.tr

Abstract. In this study, the polyamide 6 (PA) matrix was reinforced with the purified, fine ground and amino-silane treated halloysite nanotubes (HNT) at different concentrations. The preparation of composites was carried out using a lab-scale twin-screw micro-compounder with loading ratios at 0.5, 1, 3, and 20% by weight, and the test samples were prepared by the injection-molding process. According to mechanical test results, additions of HNT to the PA matrix caused slight improvements in tensile strength and Youngs' modulus parameters. The optimum concentrations for all of the additives used were estimated by comparison of mechanical test data. The addition of aminosilane-modified HNT resulted in a higher impact performance at high loading levels up to 3% concentrations. Further addition of HNT caused a reduction in the mechanical parameters of composites. Thermal studies revealed that the glass transition temperature of PA shifted to higher values after HNT mineral inclusions. Thermo-mechanical results showed that storage moduli of PA exhibited improvement with an increase in HNT content. The distributions of HNT clay into the PA phase were visualized with SEM images. Based on these observations, a high level of dispersion homogeneity was achieved for lower filling ratios. According to melt-flow and force measurements, composites filled with 20% of HNT displayed a remarkable increase in exerted force during melt-blending.

INTRODUCTION

Polyamide (PA) is an engineering thermoplastic polymer having a semi-crystalline structure. PA is classified as high-performance plastic due to its resistance to abrasive and high-temperature environments. This characteristic property makes PA favorable for numerous application fields including electronics, biomedical, transportation, and construction-related industrial areas [1-6]. Fabrication of PA-based composites leads to level up basic properties of PA in which desired mechanical and thermal conditions can be achieved for several automobile parts including body panels, wheel covers, timing belt covers, air intake manifolds, and wiring clips [7-11].

Halloysite nanotubes (HNT) are naturally occurring clay involving rolled alumina-silicate sheets with tetrahedral SiO_4 units and octahedral $AlO_2(OH)_4$ layers in their structure. HNT has unique properties owing to having a high aspect ratio (L/D) attributed to one-dimensional (1D) fibrous structure, cation exchange capacity, and low hydroxyl group density on its surface [12-14]. These characteristics make HNT suitable and economical reinforcing material for a wide variety of products ranging from building materials to anti-corrosive and flame-retardant films [15-22]. Additionally, HNT found effective use in biomedical applications such as drug delivery and anti-cancer treatments thanks to its harmless and cytotoxicity nature [23-25].

Proceedings of the 36th Conference of the Polymer Processing Society – PPS36
AIP Conf. Proc. 2607, 070005-1–070005-8; https://doi.org/10.1063/5.0135873
Published by AIP Publishing. 978-0-7354-4506-2/$30.00

The final performance of polymeric nano-composites depends on the establishment of chemical and physical interactions between the polymer phase and reinforcer material primarily. The formation of these interactions occurs in molecular dimensions for polymer nanocomposites due to the present order of nanometers scale of at least one dimension of nano-filler. Surface modification of additives is the most practical way in order to donate reactive moieties on filler surfaces. Polymer-based nanocomposites exhibit remarkable performance enhancement after the inclusion of surface-modified additives with the help of strong adhesion capacity and homogeneous dispersion [26-28].

This research study is focused on the effect of surface-modified HNT loading on the mechanical, thermal, and physical performance of PA6-based nano-composites. Composite samples were produced with four different filling ratios by the melt-blending technique. In addition to the low amount of HNT inclusions (0.5%, 1.0%, and 3.0%), the influence of the high loading level (20.0%) of HNT on the PA matrix was also investigated. Injection molding was used to prepare test samples according to related standards. Conventional processing methods were preferred in the case of composite fabrication because of economical and practical reasons in addition to easy adaptation to large-scale production. Mechanical, thermo-mechanical, thermal, and morphological investigations of PA-based nano-composites were reported to be performed via tensile, hardness, and impact tests, dynamic mechanical analysis (DMA), differential scanning calorimetry (DSC), thermal gravimetric analysis (TGA), scanning electron microscopy (SEM) method, respectively. Additionally, the processing performance of composites was evaluated with the help of melt flow index (MFI) and force measurements during melt-mixing.

MATERIALS AND METHODS

Polyamide 6 with the commercial name of Bergamid B65W25 was purchased by PolyOne Inc., USA. The commercially silane-treated HNT clay under the trade name ESH HNT 5S was supplied from Esan Eczacıbaşı Industrial Raw Materials Co., Turkey. According to producer data, each hollow tube of this HNT grade has a diameter, length, and wall thicknesses of 20-40 nm, 0.5-3.0 μm, and 0.7-1.0 nm, respectively.

PA beads and HNT powder were pre-dried at 100˚C for 2 hours before the extrusion process due to the removal of possible moisture. The fabrication of composites was carried out by a lab-scale counter-rotating twin-screw micro-compounder (MC 15 HT, Xplore Instruments). The amounts of HNT in composites are 0.5, 1.0, 3.0, and 20.0 wt.%. Composite samples were coded as PA/0.5 HNT, PA/1.0 HNT, PA/3.0 HNT, and PA/20.0 HNT, accordingly. The mixing temperature, screw speed, and mixing time interval parameters during extrusion were applied as 230˚C, 100 rpm, and 5 min, respectively. Dog-bone-shaped test specimens were obtained by injection molding instrument (Micro-injector, Daca Instruments). The barrel temperature, injection pressure, and holding time parameters throughout the molding process were used as 235˚C, 8 bar, and 3 min. Test samples have dimensions of 7.4×2.1×80 mm^3 following the ASTM D-638 standard.

Force measurements were performed during the extrusion process using the digital screen of the MC 15 HT micro-compounder. Force values were recorded in time intervals of 30 minutes using a digital chronometer.

Tensile parameters (tensile strength, percentage strain, and tensile modulus) of composites were recorded using Lloyd LR 30 K universal tensile testing device. The load cell of 5 kN and a crosshead speed of 5 cm/min were applied.

The shore hardness test was carried out by Zwick R5LB041 digital hardness tester.

The impact test was performed with a Coesfeld material impact tester using a 4J pendulum. All the results represent an average value of five samples with standard deviations.

Perkin Elmer DMA 8000 analyzer was utilized to examine the thermo-mechanical response of composites in the temperature range of -50–150°C, mode of dual cantilever bending, a constant frequency of 1Hz, and a heating rate of 10°C/min.

Thermal studies of composite samples were evaluated by TGA and DSC analyses using Netzsch Jupiter STA 449 F3 testing device. Test parameters of thermal tests were applied as a temperature range of 25˚C-600˚C, a heating rate of 10˚C/min, and a nitrogen flow of 50 ml/min.

MFI values were recorded by Coesfeld meltfixer LT under a specified standard load of 2.16 kg at the process temperature of PA (230˚C). All the results represent an average value of five samples with standard deviations.

JEOL JSM-6400 electron microscope was conducted to take SEM images of composites. Fractured surfaces of samples obtained from the impact test were coated with a thin layer of gold to achieve a conductive surface during SEM analysis.

RESULTS AND DISCUSSION

Mechanical Behaviours

Tensile test parameters of PA and composites are visualized by characteristic stress–elongation curves as displayed in Figure 1 and the relevant tensile test data are summarized in Table 1 accordingly.

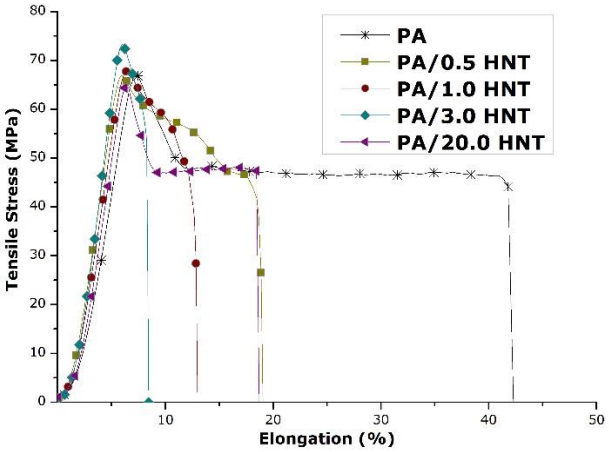

FIGURE 1. Tensile test curve of PA and PA/HNT composites

According to Figure 1, unfilled PA exhibited long-range necking behavior which is the characteristic property of ductile PA polymer. The amount of neck formation was reduced by the addition of HNT as can be observed from the tensile curves in Figure 1.

TABLE 1. Tensile test data of PA and PA/HNT composites

Sample Code	Tensile Strength (MPa)	Tensile Modulus (GPa)	Elongation at Break (%)
PA	66.8±0.5	1.5±0.1	42.1±1.3
PA/0.5 HNT	67.1±0.3	1.6±0.1	19.0±0.9
PA/1.0 HNT	68.3±0.4	1.7±0.1	12.9±0.5
PA/3.0 HNT	73.0±0.6	1.9±0.1	8.4±0.4
PA/20.0 HNT	65.0±0.5	1.5±0.1	18.6±0.7

Tensile parameters listed in Table 1 claimed that tensile strength showed an increasing trend with the additions of HNT up to 3.0% content. The greatest strength value was reached for PA/3.0 HNT candidate with a 9.3% improvement concerning the tensile strength of PA. The formation of chemical interactions between polymer-additive interfaces thanks to the silane-rich surface of HNT is responsible for these enhancements in tensile strength [29,30]. Composite involving 20.0% HNT gave decreasing in which lower tensile strength value was observed compared to pure PA. Similarly, HNT inclusions caused a slight improvement in the tensile modulus of PA. These findings are in agreement with the theoretical predictions regarding tensile modulus in literature [31-33]. Elongation of PA was affected negatively by HNT additions as described by reduction of necking behavior of PA. In other words, the PA matrix lost ductile characteristics after HNT incorporation.

The impact strength values of PA and composites are displayed in Figure 2. Impact resistance of pure PA showed an increasing trend with 0.5% concentration of HNT in which 21% enhancement was achieved. Further addition of HNT caused a reduction in impact strength values. However, PA/1.0 HNT and PA/3.0 HNT composite samples exhibited higher impact resistance relative to unfilled PA. Inclusion of HNT at lower contents led to an increase in impact energy of polymer matrix which may stem from the high aspect ratio of fibrous HNT structure. The composite containing the highest amount of HNT yielded a dramatic decrease in impact strength of unfilled PA as shown in Figure 2. This finding may be described by the stress failure formations between the highly loaded HNT and PA phase. HNT clay in extremely high content resulted in the restriction of deformation tendency of polymer matrix by causing a drop-down in the total free energy of composite [34-37].

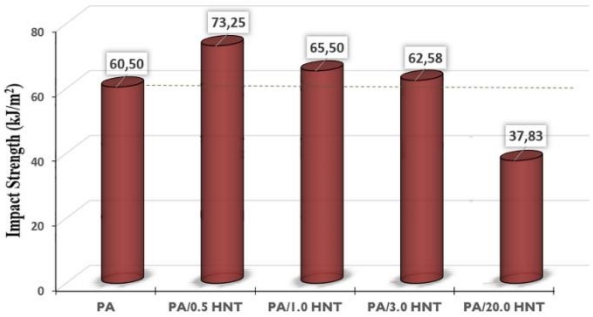

FIGURE 2. Impact test data of PA and PA/HNT composites

Shore A-type hardness values of unfilled PA and PA/HNT composites are listed in Table 2. According to these results, the hardness parameter of PA showed improvement with the adding amount of HNT. The lowest concentration of HNT gave nearly a 1.0% increase, whereas the composite having the highest content of HNT yielded a 7.5% increase concerning unfilled PA.

TABLE 2. Shore hardness measurements

Sample Code	Shore A
PA	64.0
PA/0.5 HNT	64.6
PA/1.0 HNT	65.1
PA/3.0 HNT	66.3
PA/20.0 HNT	68.8

Thermo-mechanical Response

The storage moduli and Tan δ curves as a function of temperature are displayed in Figure 3.

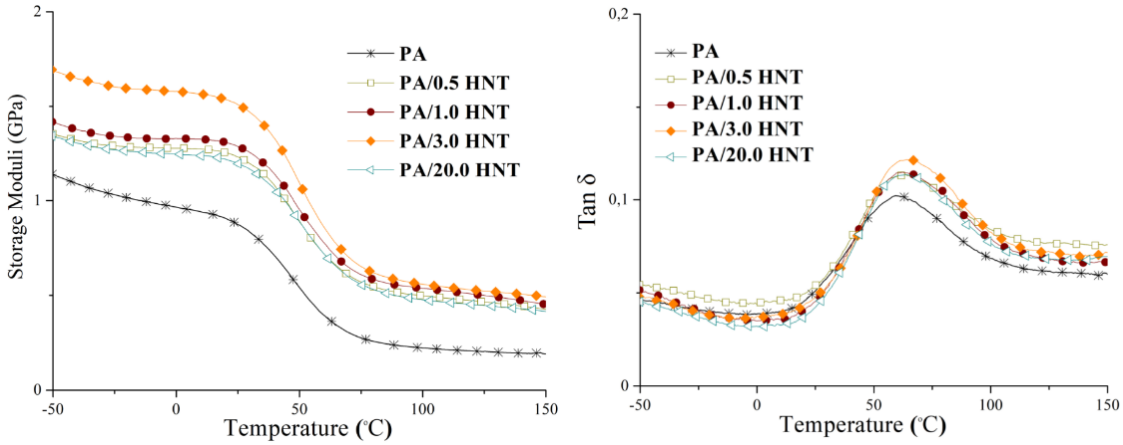

FIGURE 3. Storage moduli (a) and Tan δ (b) curves of PA and PA/HNT composites

The storage modulus of neat PA was enhanced with the inclusion of HNT regardless of concentration. The maximum modulus value was obtained for PA/3.0% HNT candidate. Similar to the tensile modulus result, 20.0% loading of HNT caused a remarkable lowering in storage modulus.

The peak value and broadening of Tan δ curve refer to the glass transition temperature (T_g) and damping property of the polymer [38-40]. According to Tan δ curves in Figure 3, HNT additions led to an increase in the T_g value of PA. Accordingly, broader curves were observed for PA/HNT composites compared to Tan δ curve of unfilled PA. This result implied that HNT inclusions donated damping behavior to the PA matrix for all of the adding amounts.

Thermal Properties

TGA and DSC curves of PA and composites are given in Figure 4a and Figure 4b, respectively. Thermal parameters including melting temperature (T_m) and decomposition temperature (T_d) are listed in Table 3.

TABLE 3. TGA and DSC parameters of PA and composites

Sample Code	Melting Point (ºC)	Decomposition Temperature (ºC)	Char Yield (%)
PA	220.0±0.2	420.5±0.3	1.2±0.1
PA/0.5 HNT	221.3±0.2	421.0±0.2	1.6±0.2
PA/1.0 HNT	221.5±0.1	421.8±0.2	1.9±0.1
PA/3.0 HNT	220.7±0.2	419.3±0.1	2.4±0.1
PA/20.0 HNT	219.6±0.1	417.1±0.3	16.5±0.2

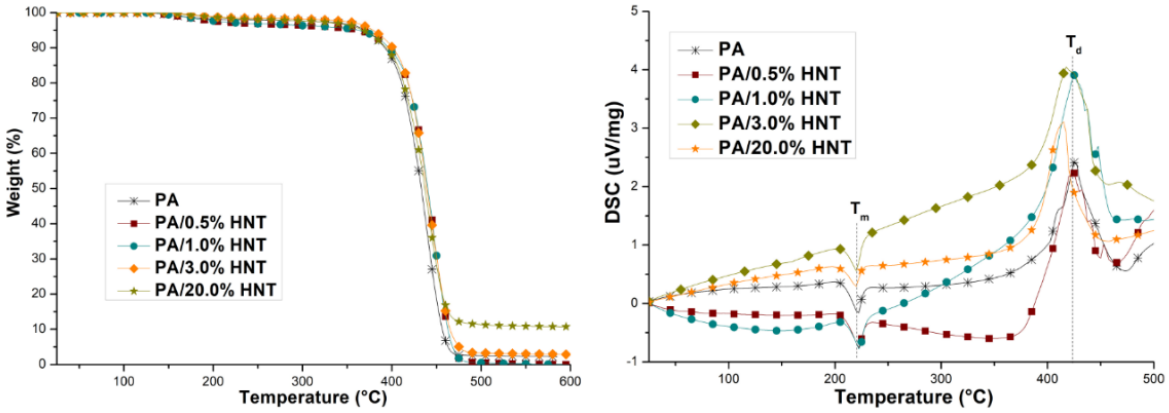

(a) (b)

FIGURE 4. TGA (a) and DSC (b) curves of PA and composites

TGA curve of neat PA in Figure 4a revealed that the weight of polymer falls out in a single step degradation. HNT additions caused shifting in degradation temperature of unfilled PA matrix. This finding is linked to an improvement in the thermal stability of the polymer phase with the help of HNT clay incorporation. The increase in thermal stability is essential for high-temperature processing steps of polymeric composites. Composite samples involving lower amounts of HNT gave nearly identical curves in addition to relatively higher shifted curves than the 20% HNT-loaded composite sample. The positive impact of the low filling ratio of HNT to thermal resistance was obtained in correlation with previous findings in the mechanical and thermo-mechanical performance of composites. Additionally, the PA/20.0% HNT candidate yielded the highest char yield as expected. It was also found that remarkable amounts of HNT clay decomposed at the end of the TGA test based on the char yield values of composites.

According to DSC curves of PA and composites shown in Figure 4b, HNT inclusions with low contents (0.5% and 1.0%) resulted in an improvement of T_m value for neat PA where nearly 1.5 units increase was observed for both composites. Conversely, composite filled with the highest loading level displayed a slightly lower T_m value than that of PA. This may be caused by the formation of HNT bundles for 20.0% adding amount of clay. Similar to T_m findings, HNT inclusions with 0.5% and 1.0% concentrations gave higher T_d values than highly HNT-loaded composites. Their decomposition temperatures were found as nearly identical to unfilled PA

The intensity and the total area of the endothermic peak in the T_m region of the DSC curve are linked to melting enthalpy related to the melting of PA segments [41,42]. Based on the DSC curves of neat PA and PA/HNT composites, the melting enthalpy of PA was not affected by the addition of HNT for low concentrations whereas, a reduction in intensity and area of the endothermic peak was obtained for PA/20.0 HNT composite which may stem from the decrease in polymer-filler interaction into PA structure.

Processing Performance

The representative graph involving force curves as a function of time is given in Figure 5.

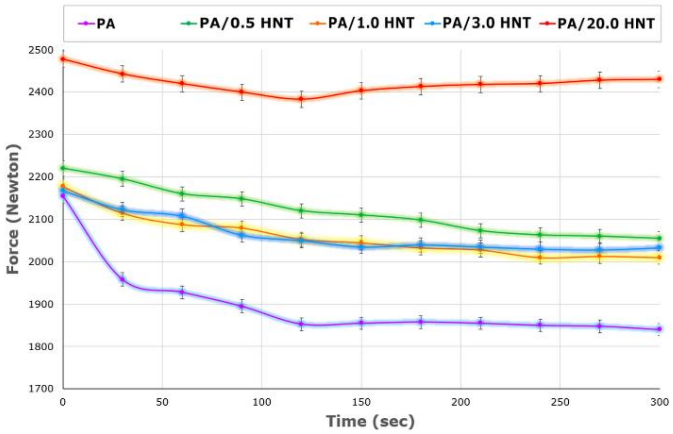

FIGURE 5. Force versus time curves of PA and PA/HNT composites

The exerted force during the extrusion process is related to the torque of screws and shear formations and this parameter is considered to be indicative of the calculation of total production cost in industrial fields. The force value of neat PA exhibited a sharp decrease in 2 minutes time intervals and it stayed constant throughout the melt-blending process. HNT incorporated PA composites gave relatively higher force values compared to PA. However, the high loading of HNT caused an obvious increase in exerted force during extrusion. The final force value of PA/20.0 HNT composite was found to be higher than unfilled PA with a factor of 75%. This result indicated that the highly-loaded HNT composite sample is not suitable for large-scale applications due to the possible cost-elevation.

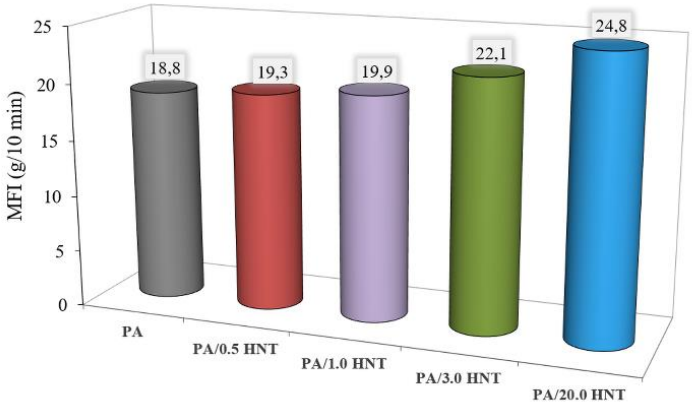

FIGURE 6. MFI parameters of PA and PA/HNT composites

Melt-flow rate is also used to evaluate the ease of processing since this parameter indicates the viscosity of the molten polymer. MFI values of PA and composites are represented in Figure 6. HNT inclusions with low amounts caused no remarkable change in the MFI of PA. On the other hand, the MFI value exhibited an increasing trend with further HNT additions. 20.0 HNT containing composite yielded the highest MFI parameter among samples. Since the relation of viscosity with MFI is conversely, it can be said that HNT additions reduced the viscosity of PA melt. Similar results are obtained in the literature regarding fibrous additives reinforced polymeric composites [43-46].

Morphology of Composites

The representative SEM images of composites are visualized in Figure 7. It can be observed that HNT particles seem to be homogeneously dispersed in the PA phase in the case of low additive contents. The reason for the observation of a high level of dispersion homogeneity in these composites is most probably the establishment of strong adhesion of HNT to PA matrix attributed to compatible silane layer on HNT surface. The SEM image of the composite containing 20.0% of HNT displayed that agglomerated regions were observed since the high amounts of HNT clay particles tend to form bundles stemming from the filler-filler interactions are favored rather than polymer-filler interactions for extremely high filling ratios. These observations provide visual evidence for previously discussed findings where improved performances were achieved for composites containing low amounts of HNT.

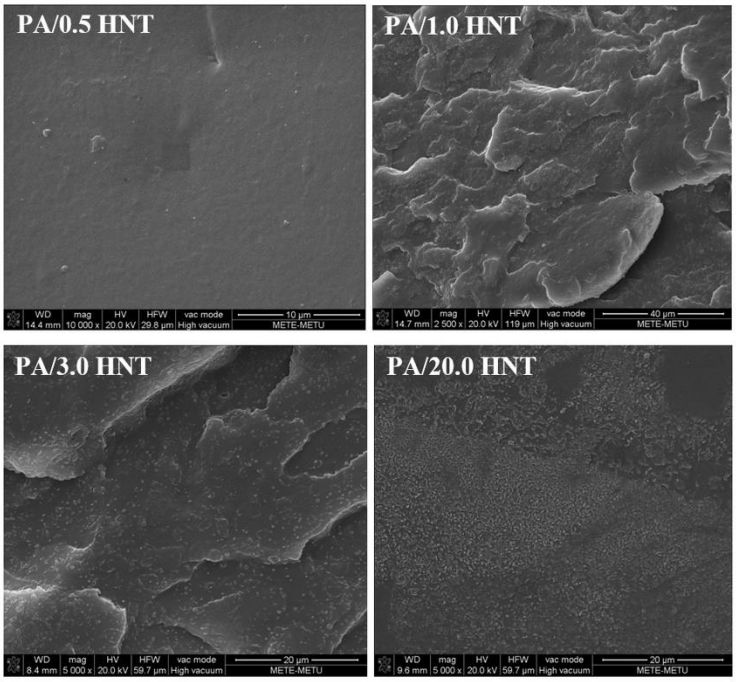

FIGURE 7. SEM images of PA/0.5 HNT (a), PA/1.0 HNT (b), PA/3.0 HNT (c), and PA/20.0 HNT (d) composites

CONCLUSIONS

In this experimental research study, the influence of HNT inclusions with various amounts on the processing, morphological, mechanical, thermal, and thermo-mechanical performance of PA6-based nanocomposites was reported. Based on the mechanical investigations, HNT additions confer tensile strength, hardness, and impact resistance in the case of low contents of HNT. Further loading of HNT resulted in dramatic reductions in the mechanical strength of composites. Thermal and thermo-mechanical analyzes revealed that unfilled PA gained thermal stability and damping behavior after the addition of HNT. Decomposition, glass transition, and melting temperature of the PA matrix also displayed increasing trends with low amounts of HNT. MFI test and force values during the melt-mixing process were evaluated to examine the processing performance of HNT-filled PA composites. MFI parameter and force value of 20% HNT loaded composite was found to be remarkably higher which indicates that high amounts of HNT exhibited a negative effect on to process conditions of composites and this sample was found to be not suitable for large-scale production considering cost-reduction affords. SEM images of composites provide proved that composites involving low content of HNT dispersed homogeneously into the PA phase in contrast to a composite containing 20% HNT in which large bundles of HNT portions were observed. According to overall results, 1.0% and 3.0% concentrations yielded higher performance among examined samples and these candidates meet industrial needs by the means of mechanical, thermal, and structural properties.

REFERENCES

1. B. L. Deopura, R. Alagirusamy, M. Joshi, and B. Gupta, *Polyesters and Polyamides* (Woodhead PublishingSawston, United Kingdom, 2008).
2. J. M. García, F. C. García, F. Serna and L. D. L. P. José, Prog. Polym. Sci. **35** (5), 623-686 (2010).
3. K. Marchildon, Macromol. React. Eng. **5** (1), 22-54 (2011).
4. J. J. Rajesh, J. Bijwe and U. S. Tewari, Wear **252** (9-10), 769-776 (2002).
5. S. Kohli and S. Bhatia, Int. J. Sci. Study **1** (1), 20-25 (2013).
6. R. Seguela, J. Polym. Sci. **58** (21), 2971-3003 (2020).
7. K. Friedrich and A. A. Abdulhakim, Appl. Compos. Mater. **20**, 107-128 (2013).
8. R. J. Varley, A. M. Groth and K. H. Leong, Polym. Int. **57**, 618-625 (2008).
9. L. Gendre, J. Njuguna, H. Abhyankar and V. Ermini, Mater. Design **66**, 486-491 (2015).
10. C. Zhang, e-Polymers **18**, 373-408 (2018).
11. B. Ravishankar, S. K. Nayak and M. A. Kader, J. Reinf. Plast. Compos. **38**, 835-845 (2019).
12. P. Yuan, D. Tan and F. Annabi-Bergaya, Appl. Clay Sci. **112**, 75-93 (2015).
13. R. Kamble, M. Ghag, S. Gaikawad, and B. K. Panda, J. Adv. Sci. Res. **3** (2), 25-29 (2012).
14. E. Joussein, S. Petit, J. Churchman, B. Theng, D. Righi and B. Delvaux, Clay Miner. **40**, 383-426 (2005).
15. Y. Lvov, W. Wang, L. Zhang and R. Fakhrullin, Adv. Mater. **28** (6), 1227-1250 (2016).
16. M. Liu, Z. Jia, D. Jia, and C. Zhou, Prog. Polym. Sci. **39** (8), 1498-1525 (2014).
17. M. Du, B. Guo and D. Jia, Polym. Int. **59** (5), 574-582 (2010).
18. E. S. Goda, K. R. Yoon, S. H. El-sayed and S. E. Hong, Thermochim. Acta **669**, 173-184 (2018).
19. C. I. Idumah, A. Hassan, J. Ogbu, J.U. Ndem and I.C. Nwuzor, Compos. Interface. **26** (9), 751-824 (2019).
20. K. A. Zahidah, S. Kakooei, M. C. Ismail and P. B. Raja, Prog. Org. Coat. **111**, 175-185 (2017).
21. R. Bouaziz, K. Prashantha and F. Roger, Mech. Adv. Mater. Struct. **26** (14), 1209-1217 (2019).
22. D. Papoulis, Appl. Clay Sci. **168**, 164-174 (2019).
23. M. Fizir, P. Dramou, N. S. Dahiru, W. Ruya, T. Huang and H. He, Microchim. Acta **185** (8), 389 (2018).
24. M. Hanif, F. Jabbar, S. Sharif, G. Abbas, A. Farooq and M. Aziz, Clay Miner. **51** (3), 469-477 (2016).
25. D. Rawtani and Y. K. Agrawal, Rev. Adv. Mater. Sci. **30** (3), 282-295 (2012).
26. S. Fu, Z. Sun, P. Huang, Y. Li and N. Hu, Nano Mater. Sci. **1** (1), 2-30 (2019).
27. L. H. Mancini and C. L. Esposito, *Nanocomposites Preparation, Properties and Performance* (Nova Science Publishers, New York, 2008).
28. J. B. Donnet., Compos. Sci. Technol. **63**, 1085-1088 (2013).
29. S. T. Mohamed, S. Tirkes, A. O. Akar and U. Tayfun, Clay Miner. **55** (4), 281-292 (2020).
30. L. Jiang, C. Zhang, M. Liu, Z. Yang, W. W. Tjiu and T. Liu, Compos. Sci. Technol. **91**, 98-103 (2014).
31. M. Moghri, S. I. S. Shahabadi and M. Madic, J. Vinyl Addit. Technol. **22** (1), 29-36 (2016).
32. Y. Zare, K. Y. Rhee and S. J. Park, Colloid. Surf. A: Physicochem. Eng. Asp. **628**, 127330 (2021).
33. M. Shahriari-Kahkeshi M. and M. Moghri, e-Polymers **17**, 187-198 (2017).
34. O. Yildirimkaraman, U. H. Yildiz, A. O. Akar and U. Tayfun, IOP SciNotes **1**(2), 024804 (2020).
35. M. Has, A. Erdem, L. A. Savas, U. Tayfun and M. Dogan, J. Thermoplast. Compos. Mater. DOI: 10.1177/08927057221096656 (2022).
36. S. C. Tjong, S. A. Xu and Y. W. Mai, Mater. Sci. Eng. A **347**, 338-345 (2003).
37. A. O. Akar, U. H. Yildiz and U. Tayfun, Rev. Adv. Mater. Sci. **60** (1), 293-302 (2021).
38. B. Wunderlich, *Thermal Analysis of Polymeric Materials* (Springer-Verlag, Berlin, 2005).
39. U. Tayfun and A. O. Akar, *The use of fullerene in thermoplastic matrices on polymeric composites applications* In *Advances in Materials Science Research* (Nova Science Publishers, New York, 2021).
40. A. Burgoa, R. Hernandez and J. L. Vilas, Polym. Int. **69** (5), 467-475 (2020).
41. Y. P. Khanna, W. P. Kuhn and W. J. Sichina, Macromol. **28**, 2644-2646 (1995).
42. V. M. Yilmaz, T. T. Parlak and K. Yildiz, J. Therm. Anal. Calorim. **134** (1), 135-141 (2018).
43. K. S. Jang, Polymer **147**, 133-141 (2018).
44. C. Arslan and M. Dogan, J. Compos. Mater. **53** (17), 2465-2475 (2019).
45. A. L. Slonov, I. V. Musov, A. Zhansitov, D. M. Khakulova, E. V. Rzhevskaya and S. Y. Khashirova, Key Eng. Mater. **816**, 48-54 (2019).
46. M Barczewski, D. Matykiewicz, O. Mysiukiewicz and P. Maciejewski, J. Polym. Eng. **38** (3), 281-289 (2018).